J. Synchrotron Rad. (1998). **5**, 1357–1362

High-Frequency X-ray Beam Chopper Based on Diffraction by Surface Acoustic Waves

R. Tucoulou,[a]* D. V. Roshchupkin,[b] O. Mathon,[a] I. A. Schelokov,[b] M. Brunel,[c] E. Ziegler[a] and C. Morawe[a]

[a]ESRF, BP 220, 38043 Grenoble CEDEX 9, France, [b]Institute of Microelectronics Technology, Russian Academy of Sciences, 142432 Chernogolovka, Moscow District, Russia, and [c]Laboratoire de Cristallographie, CNRS, BP 166, 38042 Grenoble CEDEX 9, France. E-mail: tucoulou@esrf.fr

(*Received 26 March 1998; accepted 16 June 1998*)

The diffraction of an X-ray beam on an ultrasonic wave propagating at the surface of a crystal gives rise to diffraction satellites whose temporal structure is correlated to that of the ultrasonic wave. By matching the temporal structure of the surface acoustic wave with the filling mode of the storage ring, it is possible to select or reject the incident X-ray pulses. A few examples of the performance of this MHz-range chopper for various filling modes are presented.

Keywords: surface acoustic waves; X-ray diffraction; X-ray beam chopper.

1. Introduction

The pulsed character of synchrotron radiation has been extensively used to develop time-resolved studies in many fields (Munro & Schwenter, 1983; Zarka *et al.*, 1988; Coppens, 1997; Moffat, 1996). The temporal structure of synchrotron radiation is such that a time resolution of the order of 100 ps can be achieved. However, one of the main problems in this kind of experiment is that the natural time structure of the beam (fixed by the filling mode of the electron bunches in the storage ring) may not be optimal for the study of any time-dependent system. According to the investigated phenomenon and mainly to its characteristic time (lifetime of an excited state, for example), there exists an 'ideal' time structure for the X-ray probe, which is often quite different from the intrinsic structure of synchrotron radiation. For example, time-resolved Laue diffraction on laser-excited macromolecular crystals requires approximately one short X-ray pulse per second (Wulff *et al.*, 1997) whereas time-resolved X-ray magnetic circular dichroism needs one pulse per microsecond (Bonfim *et al.*, 1998). Due to the large number of experiments installed around a synchrotron facility, the filling mode cannot be chosen to match a single specific experiment.

It is therefore necessary to match the time structure of the X-ray beam to the requirements of the experiment by selecting or rejecting the incoming X-ray pulses on the sample. This can be performed by inserting along the beam path a device called a chopper. Up to now, a few mechanical choppers have been developed (Legrand *et al.*, 1989), consisting of a high-speed rotating slotted wheel. Typical rotational speeds for current mechanical choppers are 20000 r.p.m. A mechanical chopper has been installed on ID9 at the ESRF, rotating at a frequency of 900 Hz and synchronized to a bunch clock delivered by the RF cavity of the storage ring (Wulff *et al.*, 1997). A single-slot wheel phase matched to the storage ring can transmit one X-ray pulse every 3.3 ms. The attenuated X-ray flux transmitted through the wheel can be decreased to 0.1% of that passing through the slot by choosing a high-Z material and an adequate thickness. The advantages of this chopper include a high efficiency for the transmitted X-ray pulses through the slot and possible operation with a white beam.

We present in this article a new kind of chopper based on the diffraction of X-rays by surface acoustic waves.

2. X-ray diffraction by surface acoustic waves

The interaction of X-rays with surface acoustic waves (SAWs) has already been studied and presented earlier in several articles (Roshchupkin *et al.*, 1992, 1995; Roshchupkin & Brunel, 1993). In brief, an X-ray beam reflected by a mirror excited by SAWs is diffracted by the periodic modulation formed at the mirror surface. According to the grating equation (1), constructive interferences may occur in the reflected field resulting in diffraction satellites located around the specular reflected beam. They are found at angular directions given by the grating equation,

$$\cos\alpha_m = (m\lambda/\Lambda) + \cos\alpha_0, \qquad (1)$$

where α_0 is the incident angle, α_m is the emergent angle of the mth-order satellite, λ is the X-ray wavelength and Λ is the acoustic wavelength. The travelling SAW acts as a dynamical grating, the acoustic amplitude being of the

order of 15 Å and the wave propagating at a velocity of 3500 m s^{-1}.

The rise of satellite peaks around the specular reflected beam happens in several diffraction situations: total external reflection (Roshchupkin *et al.*, 1992; Roshchupkin & Brunel, 1993), Bragg diffraction on a multilayer deposited on the vibrating surface (Roshchupkin *et al.*, 1997), or Bragg diffraction on a vibrating crystal (Tucoulou *et al.*, 1999). In the second case, the multilayer mirror follows the shape of the substrate surface and satellites rise up around the Bragg diffraction peak. About 25% of the direct beam intensity may be transferred into a desired satellite (Roshchupkin *et al.*, 1997). This configuration was chosen for the electro-acoustic chopper (see Fig. 1) and will now be described.

The most common way of exciting high-amplitude SAWs consists of using a piezoelectric substrate on which an interdigital acoustic transducer is deposited by photolithography. In our case, the piezoelectric substrate is an $LiNbO_3$ monocrystal (300 oriented) with an r.m.s. surface roughness of the order of 5 Å. The interdigital transducer has a resonance frequency of 288 MHz.

A part of the piezoelectric surface is covered with a multilayer mirror composed of 60 W/Si layers, the bilayer spacing being 47 Å. The peak reflectivity of this multilayer is about 42% at 8 keV for a Bragg angle of 0.94°. It should be noted that this reflectivity is far below the classical performances achieved by X-ray multilayer mirrors ($\geq$70%) at this energy. This difference is certainly due to the unusual substrate ($LiNbO_3$) whose surface preparation is not yet well known. Obviously, it has to be improved to achieve better results for the chopper.

Fig. 2 shows an example of a rocking curve for this multilayer modulated or not by SAWs. Three 'acoustic' diffraction orders can be seen. By using equation (1), the angular deviation of the $m = -1$ satellite with respect to the $m = 0$ order beam, for an acoustic wavelength of 12 μm, an X-ray energy of 8 keV and an incident angle of 0.94°, is $\Delta\alpha = 0.044°$. However, this cannot be directly observed on the x axis of Fig. 2; the emergent angle with respect to the surface has first to be deduced.

As mentioned above, the propagation of an SAW modulates the shape of the multilayer mirror, which can be seen as a dynamical grating. By switching on and off the electric signal fed to the transducer, SAW pulses are emitted and therefore several gratings propagate successively along the multilayer mirror. The principle is sketched in Fig. 1. Diffraction satellites appear only when an acoustic pulse crosses the beam footprint on the multilayer. Between the acoustic pulses, the surface remains flat and no satellite is produced. In conclusion, the temporal structure of the satellite radiation can therefore be pulsed and is electronically tunable.

Since the synchrotron radiation is also pulsed, the basic idea of the chopper consists of emitting acoustic pulses in such a way that they reach the beam footprint simultaneously with the selected X-ray pulses. About 20% of each of these pulses will be diffracted through the first-order satellite. All the other X-ray pulses hit a flat surface (if the X-ray interpulse period is large enough to allow time for the acoustic pulses to leave the beam footprint) and thus are diffracted in the specular direction.

Fig. 3 presents two detector scans made with and without SAWs for the optimal incident angle ($\theta_{inc} = 0.912°$) with

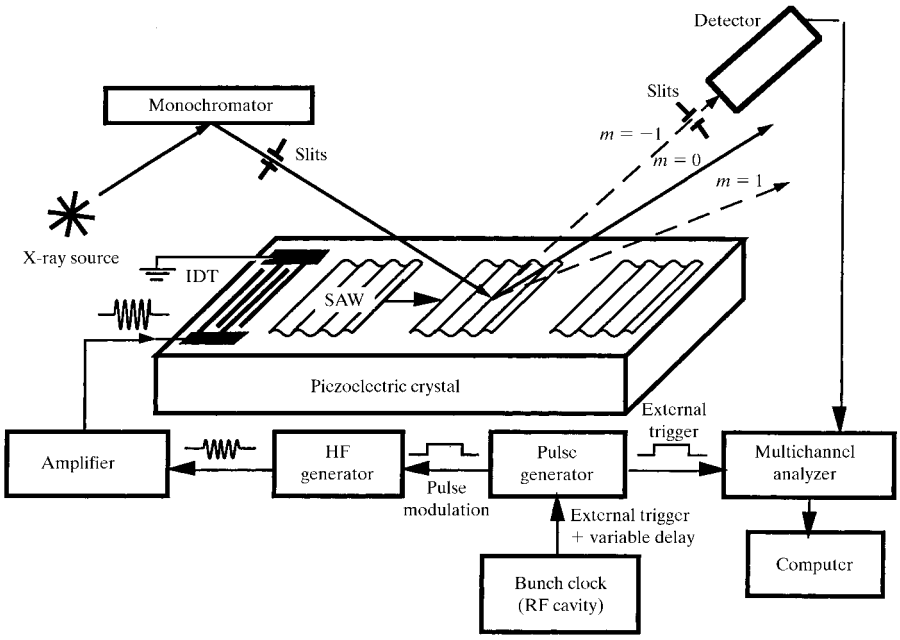

Figure 1
Principle of X-ray diffraction by a surface acoustic wave.

respect to the $m = -1$ diffraction order intensity. This intensity amounts to 50% of the exact Bragg peak intensity, *i.e.* 21% of the direct beam (the use of a high-quality multilayer would increase this value).

3. Electro-acoustic chopper

3.1. *Synchronization*

Testing the electro-acoustic chopper requires two different synchronizations: (i) it is necessary to synchronize the arrival time of the acoustic pulses on the beam footprint with respect to the X-ray pulses which must be transmitted; (ii) counting electronics (to record the satellite intensity *versus* time) have to be synchronized with the X-ray pulses since it is necessary in most cases to sum data collected from several X-ray pulses to obtain reasonable signal-to-noise ratios.

Synchronizing the external equipment to the emitted X-ray pulses is usually achieved by use of a clock pulse signal delivered by the radio-frequency accelerating system of the synchrotron ring and whose stability is rigorous (10^{-7}). The orbital period of the storage ring is exactly equal to the period of this signal. It is used to trigger a pulse generator which modulates (logical modulation) the HF signal (288 MHz) sent to the acoustic transducer. The shape of the electric rectangular pulse emitted by the pulse generator is chosen with respect to the desired characteristics (length and frequency) of the acoustic pulses.

Counting electronics are synchronized in a similar fashion. The signal coming out from the pulse generator triggers a time multichannel analyzer (MCA) composed of 1024 channels of 20 ns each with no dead time in between. The output of a scintillation detector (after amplification and discrimination in a single-channel analyzer) is fed to the MCA, which dates the arrivals of electric pulses corresponding to detected photons. After a sweep, the MCA waits for the next trigger and stores the data in memory.

3.2. *Chopper in the hybrid mode*

This chopper was tested with the storage ring filled in the so-called hybrid mode (Tucoulou *et al.*, 1997). Electron bunches are asymmetrically spaced: 350 bunches (described as a 'superpulse') are injected closely spaced and occupy one-third of the ring (total intensity 140 mA), and a single bunch (7 mA) is placed diametrically opposite to them. It has been shown that this chopper was able to select each single X-ray pulse and to remove all the 'superpulses', thus delivering a beam with a temporal structure similar to a single-bunch mode. To illustrate the flexibility of this chopper, we present in Fig. 4 another mode of selection. Only one superpulse out of four is selected in the direction of the first-order satellite: after the chopper, the temporal structure of the beam consists of superpulses (350 closely spaced pulses) separated by 11.28 μs. In this experiment, the direct beam was collimated by slits of dimensions 50 μm in the vertical plane and 1 mm in the horizontal plane. The MCA does not have enough resolution to separate each pulse within the superpulse. The irregular shape of the large pulses in Fig. 4 may be due to pile-up problems but their integrated intensity remains constant.

The acoustic pulses were 0.8 μs long and their frequency was one-quarter of the orbital frequency, *i.e.* 89 kHz. The time period between the lone pulse and the close-spaced ones was 0.9 μs, which was sufficient for the acoustic pulse to entirely leave the illuminated zone before the arrival of the following unwanted X-ray pulses.

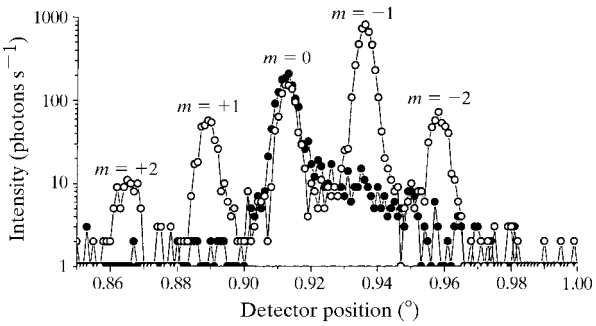

Figure 3
Detector scans with (empty circles) and without (filled circles) surface acoustic waves. $E = 8$ keV. $f = 288$ MHz.

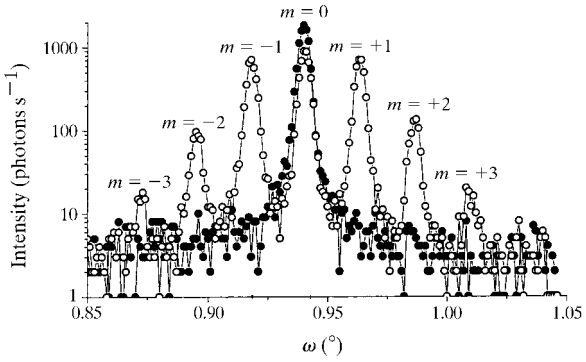

Figure 2
Rocking curves with (empty circles) and without (filled circles) surface acoustic waves. $E = 8$ keV. $f = 288$ MHz.

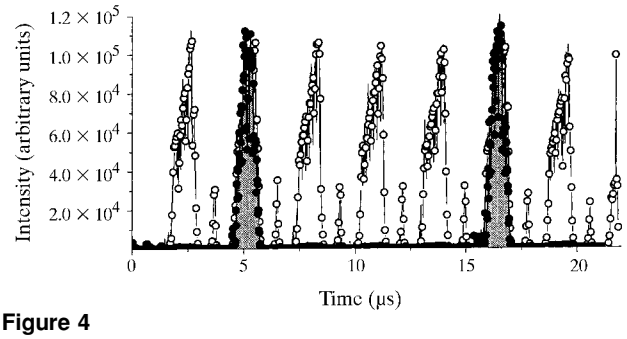

Figure 4
$m = +1$ order satellite intensity *versus* time in the hybrid mode. Empty circles: unpulsed mode. Filled circles: pulsed mode. One superpulse out of four is selected.

3.3. *Chopper in the 16-bunch mode*

Fig. 5 presents the intensity recorded in the +1 satellite direction as a function of time for another filling mode of the storage ring, namely the 16-bunch mode (16 equally spaced bunches around the ring). The chopper modulation was set to select X-ray pulses during 8 μs and then to stop those arriving during the following 3 μs.

A single X-ray burst has a duration of the order of 50 ps. It is not surprising to see at least six excited channels for one single burst, *i.e.* 120 ns (see insert in Fig. 5), since the electronic detection of photons is based on the detection of maxima of electric pulses emitted by a scintillation detector. The error on this detection is of the order of 100 ns and explains the large number of excited channels. Nevertheless, the 16-bunch structure (50 ps pulses separated by 176 ns) could still be resolved.

3.4. *Chopper in the single-bunch mode*

In this mode, X-ray pulses are delivered at a frequency of 355 kHz. We used this mode to evaluate the selection/rejection efficiency of our electro-acoustic chopper. The energy was set to 12 keV and the beam size was 0.05 × 1 mm. The acoustic pulses had a duration of 1 μs which was enough to cover the beam footprint (approximately 5 mm for a Bragg angle of 0.6°) and they were separated by 1.8 μs, which was adequate for each acoustic pulse to leave the footprint area before the arrival of the next X-ray pulse and consequently to select one pulse out of two.

Fig. 6 presents the results of this experiment. Fig. 6(*a*) gives the time structure of the $m = +1$ diffraction order in the case of a travelling SAW without pulsation (continuous wave). Here, all the X-ray pulses are selected. For Fig. 6(*b*), the pulsation mode is on and one pulse out of two is selected. The Bragg efficiency of this multilayer is of the order of 40% and, as seen in Fig. 2, the $m = +1$ diffraction order can reach 50% of the Bragg peak, resulting in the transmission in the diffraction satellite of 20% of the direct intensity.

The pulse integrated intensity is identical for pulsed or continuous travelling waves indicating that the entire X-ray beam footprint was under acoustic modulation when the X-ray pulses arrived, and that the relative phasing between the acoustic and the X-ray pulses was correctly adjusted.

For the user, the relevant figure of merit for this device is the signal-to-noise ratio in the diffraction satellite defined as the beam intensity after the chopper divided by the intensity contribution still transmitted in the satellite by the unwanted pulses. A signal-to-noise ratio of 60 was measured. This is one of the limitations of the electro-acoustic chopper which has to be improved. It is very important to obtain a rejection rate of the unwanted pulses as high as possible, especially if many of them have to be removed. The origin of the important noise level should be found in the quality of the multilayer. As the tails of the Bragg peak spread over a large angular range, a non-negligible intensity is observed at the position of the first-order satellite located 0.04° away from the Bragg peak. Consequently, in the absence of an acoustic pulse, instead of being ideally equal to zero the diffused intensity was measured to be as high as 1% of the satellite intensity.

3.5. *Double electro-acoustic chopper*

One way of decreasing this background diffusion is to add a second electro-acoustic device immediately after the first one (see Fig. 7 for the experimental set-up). The X-ray pulses (and the noise) are diffracted through the $m = +1$ satellite of the first device and then rediffracted by the second one on which the acoustic pulses are emitted to reselect the pulses transmitted by the first one. The results

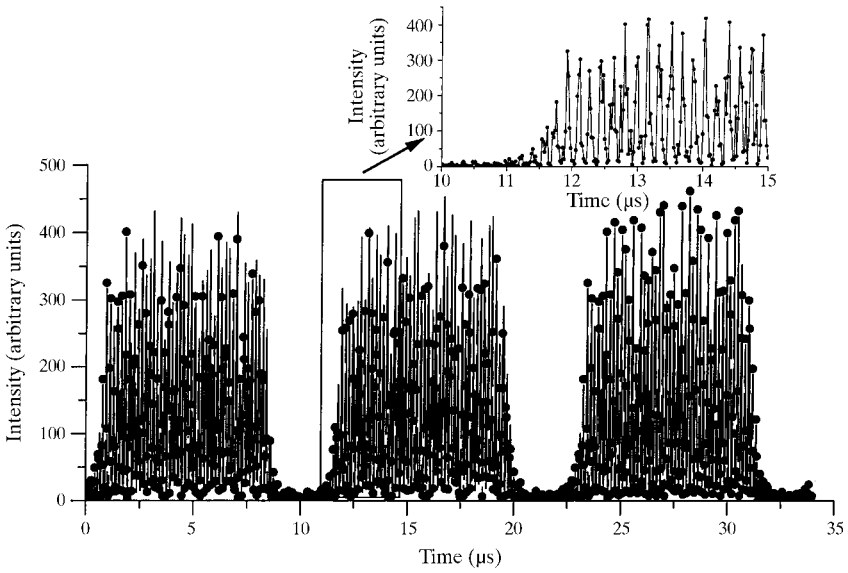

Figure 5
$m = +1$ order satellite intensity *versus* time in the 16-bunch mode. About 45 X-ray pulses are selected every 11 μs.

are shown in Fig. 8. The intensity of the $m = -1$ diffraction order of the second chopper is recorded as a function of time. Fig. 8(*a*) shows the twice-diffracted intensity when both choppers work in a non-pulsed mode (each X-ray pulse is selected). Fig. 8(*b*) shows this intensity when only the first chopper is pulsed. Fig. 8(*c*) corresponds to the double-pulsed mode. In this case, the selection efficiency was of the order of 3 or 4% with respect to the direct beam intensity. The signal-to-noise ratio was decreased to 400. Unfortunately, the quality of the second multilayer was worse than for the first one; the expected value for the signal-to-noise ratio should have been $60^2 = 3600$ in the case of two identical multilayers. Nevertheless, the advantage of this association was demonstrated. In addition, as the second mirror exactly compensates the angular deviation produced by the first mirror, this set-up preserves the direction of the incident X-ray beam.

4. Limitations

There are temporal limitations related to the size of the direct beam and the Bragg angle of the multilayer. These two parameters influence the size of the beam footprint on the surface and, hence, the propagation time needed by an acoustic pulse to cross it. Since the SAW velocity is 3500 m s^{-1}, a pulse requires 1 μs to propagate 3.5 mm along the surface. In our experiment (Bragg angle 0.6°, beam width 50 μm) the footprint reached about 5 mm and it required at least 1.5 μs for an acoustic pulse to propagate along this area. Therefore, two close X-ray pulses (less than 1.5 μs in between) cannot be separated by the present set-up. Both will see a modulated surface and will be partially diffracted through the satellite. For this reason, it is not yet possible to extract one single X-ray pulse in the 16-bunch mode at 12 keV for a reasonable beam size (∼50 μm and more). Possible means of increasing the selection frequency include the use of a Bragg reflection of the piezoelectric crystal itself since the incident angles are much higher (about 20° at 12 keV).

The operation with a monochromatic beam (or with an energy bandpass smaller than the acceptance of the multilayer) is another limit.

With the present set-up, only 20% of the direct beam was diffracted through the first diffraction order. The reflectivity of the multilayers we used in our tests was far below the performance that has been achieved at this energy with X-ray multilayer mirrors deposited on silicon substrates. The multilayer quality could definitely be improved if better substrates were available. To our knowledge, it is the first time that an $LiNbO_3$ substrate had been used for depositing X-ray multilayers. Efforts are now in progress to obtain $LiNbO_3$ substrates with better specifications regarding surface roughness and planarity. At an energy of 12 keV, a peak reflectivity in excess of 70% is expected.

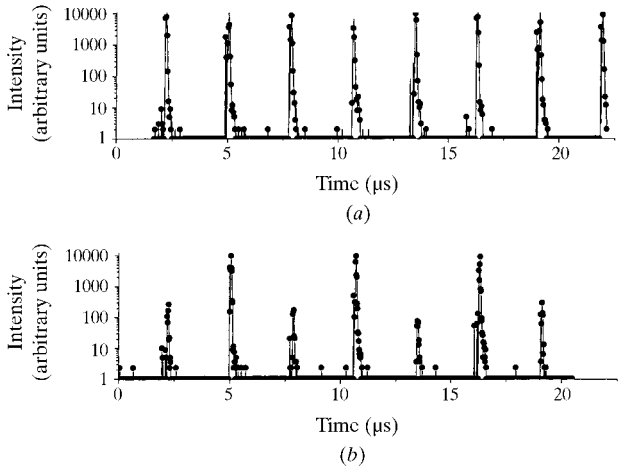

Figure 6
$m = +1$ order satellite intensity *versus* time in the single-bunch mode. (*a*) Unpulsed mode. (*b*) Pulsed mode. One pulse out of two is selected.

5. Conclusions

We have presented here an X-ray beam chopper based on diffraction by SAWs. Basically, this electro-acoustic chopper consists of an SAW device (acoustic frequency ≃ 300 MHz) partially covered with a multilayer mirror, an HF generator, a goniometer to hold the SAW device and synchronizing electronics.

It has been proved that since the wave-form shaping of the acoustic pulses is very easy to perform, this system is very flexible and could thus satisfy users who require radically different temporal structures. Up to now, this chopper can select 20% of X-ray pulses in the MHz range.

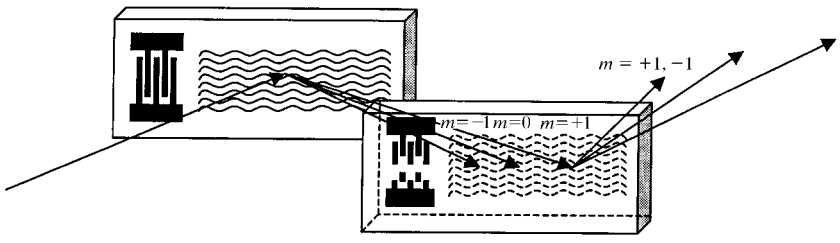

Figure 7
Double electro-acoustic chopper scheme. The Bragg condition of the second multilayer is only fulfilled for the $m = +1$ satellite. The $m = +1, -1$ satellite is selected at the output of the chopper.

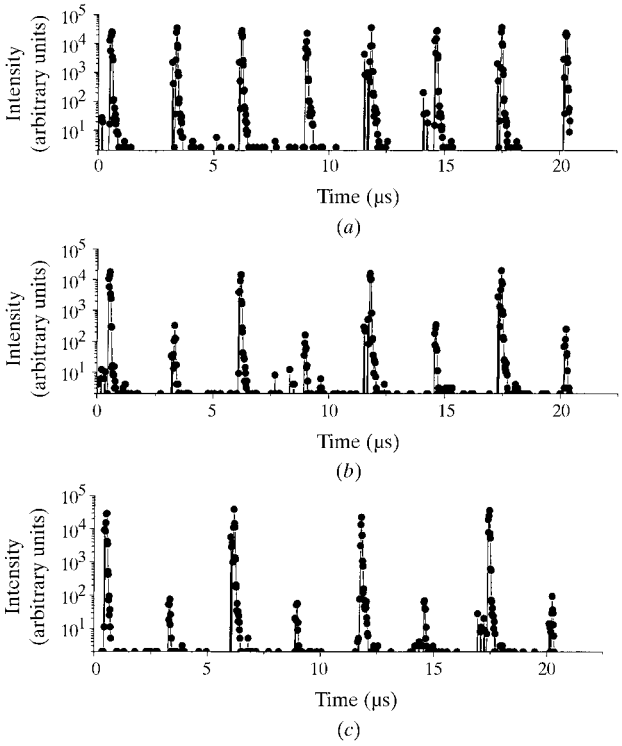

Figure 8
Double electro-acoustic chopper. (*a*) Unpulsed mode on the two choppers. (*b*) First chopper pulsed, second chopper unpulsed. (*c*) Pulsed mode on the two choppers.

It should be noted that by sending a single acoustic pulse this system could work as a fast shutter in the microsecond range.

The present study has been supported by an INTAS project (93-1711), by a NATO Linkage Grant (921337) and by a PICS project (CNRS). Patent number: 9703031.

References

Bonfim, M., Mackay, K., Pizzini, S., San Miguel, A., Tolentino, H., Giles, C., Neisius, T., Hagelstein, M., Baudelet, F., Malgrange, C. & Fontaine, A. (1998). *J. Synchrotron Rad.* **5**, 750–752.
Coppens, P. (1997). *Synchrotron Rad. News*, **10**(1), 26–30.
Legrand, A. D., Schildkamp, W. & Blank, B. (1989). *Nucl. Instrum. Methods*, A**275**, 442–446.
Moffat, K. (1996). *Synchrotron Rad. News*, **9**(6), 15–18.
Munro, I. H. & Schwenter, N. (1983). *Nucl. Instrum. Methods*, **208**, 819–834.
Roshchupkin, D. V. & Brunel, M. (1993). *Rev. Sci. Instrum.* **64**, 379–382.
Roshchupkin, D. V., Brunel, M., de Bergevin, F. & Erko, A. I. (1992). *Nucl. Instrum. Methods*, B**72**, 471–476.
Roshchupkin, D. V., Schelokov, I. A., Tucoulou, R. & Brunel, M. (1995). *IEEE Trans. Sonics Ultrasonics*, **42**(1), 127–134.
Roshchupkin, D. V., Schelokov, I. A., Tucoulou, R. & Brunel, M. (1997). *Nucl. Instrum. Methods*, B**129**, 414–418.
Tucoulou, R., Roshchupkin, D. V., Schelokov, I. A., Brunel, M., Ortega, L., Ziegler, E., Lingham, M., Mouget, C. & Douillet, S. (1997). *Nucl. Instrum. Methods*, B**132**, 207–213.
Tucoulou, R., Roshchupkin, D. V., Schelokov, I. A., Mathon, O. & Brunel, M. (1999). In preparation.
Wulff, M., Schotte, F., Naylor, G., Bourgeois, D., Moffat, K. & Mourou, G. (1997). *Nucl. Instrum. Methods*, A**398**, 69–84.
Zarka, A., Capelle, B., Detaint, J. & Schwartzel, J. (1988). *J. Appl. Cryst.* **21**, 967–971.